Electrical Power and Energy Systems 156 (2024) 109711

Contents lists available at ScienceDirect

International Journal of Electrical Power and Energy Systems

journal homepage: www.elsevier.com/locate/ijepes

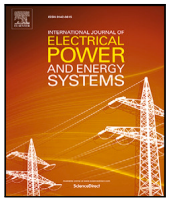

Enhancing grid protection: The crucial role of resistive-type superconducting fault current limiters in transmission line current differential relays

Qihuan Dong [a,*], Haozong Wang [a], Binshu Chen [a], Ning Zhang [a], W.T.B. de Sousa [b], Yilu Liu [c]

[a] Tsinghua University, Electrical Engineering Department, Beijing, 100084, China
[b] Institute for Technical Physics, Karlsruhe Institute of Technology, Eggenstein-Leopoldshafen, 76344, Germany
[c] The University of Tennessee, Department of Electrical Engineering and Computer Science, Knoxville, 37996, TN, USA

ARTICLE INFO

Keywords:
Current differential protective relaying
High temperature superconductors
Protective relays
Superconducting fault current limiters
Transmission systems
Thermal electric analogy

ABSTRACT

Superconducting fault current limiters (SFCLs) offer an efficient means of limiting fault currents and supporting system reliability. However, they weaken the fault characteristics and reduce the sensitivity of traditional relay protection. The seamless integration of SFCLs with protective relays remains a complex and under-explored area, impeding their widespread industrial adoption. In parallel, current differential protective (CDP) relays are almost the primary protection for all high-voltage electrical equipment and are the cornerstone of global power system security. This paper fills a critical knowledge gap by researching the intricate interaction between resistive superconducting fault current limiters (R-SFCLs) and current differential protective relays. Our investigation commences with a comprehensive mathematical analysis, while researching the influence of R-SFCLs on CDP operation. Subsequently, we conduct a series of comparative experiments using the Matlab Simulink software platform. These tests evaluate the sensitivity, dependability, and security of CDPs in scenarios with and without R-SFCLs. The simulation results not only confirm the accuracy of our analytical framework but also shed light on the multifaceted relationship between R-SFCLs and CDPs. This research contributes to a deeper understanding of how R-SFCLs can be effectively integrated into power systems, offering a roadmap for enhancing grid protection.

1. Introduction

In modern power systems, managing escalating short-circuit currents is increasingly crucial. Superconducting fault current limiters (SFCLs) offer a viable solution to mitigate these issues while maintaining grid stability, efficiency, and responsiveness [1,2]. SFCLs operate with minimal impedance under normal operating conditions, yet provide substantial impedance in the event of faults, thereby effectively curtailing fault currents [3].

The development and deployment of SFCLs are being actively pursued globally, with significant projects and initiatives in Europe, Korea, China, and other regions, illustrating the widespread interest in this technology [4–12]. However, the integration of SFCLs into existing power systems, particularly their coordination with protective relays, poses substantial challenges [13–16].

Protective relays, especially current differential protective relays (CDPs), play a pivotal role in ensuring the safe operation of power systems [17]. The introduction of SFCLs can significantly alter the electrical parameters, such as current and voltage, potentially leading to mal-operation or mis-operation of these relays. This paper focuses on the coordination between resistive-type SFCLs (R-SFCLs) and CDPs.

CDP relays are widely used protective relays known for their superior security [18]. They respond only to faults within predefined zones, thereby enhancing grid reliability. R-SFCLs are among the most developed SFCL types, owing to their simplicity and commercial maturity [19]. However, the coordination of line current differential protection with R-SFCLs remains under-explored. Therefore, researching the coordination between R-SFCLs and CDP relays is crucial. This exploration focuses on understanding the complex interactions between these two systems. The objective is to optimize R-SFCLs for effective short-circuit current limitation while ensuring CDP relays maintain optimal sensitivity and accuracy. Achieving this integration could significantly improve the electrical system's performance. It also ensures that the system can respond promptly and accurately in the event of a fault, minimizing damage and guaranteeing reliable operation of the power grid.

This paper aims to analyze the impact of R-SFCLs on line current differential protection, specifically evaluating their dependability and sensitivity in internal fault scenarios and their security in external fault scenarios [20]. The study utilizes a combination of quantitative analysis

* Corresponding author.
E-mail address: qd210cam@163.com (Q. Dong).

https://doi.org/10.1016/j.ijepes.2023.109711
Received 30 October 2023; Received in revised form 26 November 2023; Accepted 5 December 2023
Available online 14 December 2023

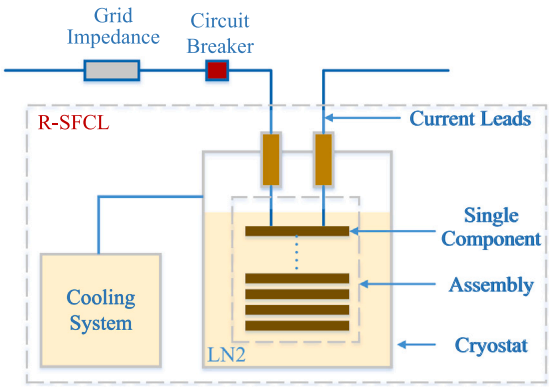

Fig. 1. Block diagram of an R-SFCL.

and numerical simulations to provide insights into this crucial aspect of power system protection.

The paper is structured as follows: Section 2 introduces the fundamentals and modeling of R-SFCLs. In Section 3, we explore the working principles of CDPs, establishing a foundational understanding of their interactions with R-SFCLs. Section 4 presents a comprehensive quantitative analysis, examining the impact of R-SFCLs on CDPs and offering detailed insights into their operational dynamics. This is followed by a practical case study within a transmission system in Section 5. The paper concludes with Section 6.

2. Modeling and working principle of R-SFCLs

2.1. Working principles of the R-SFCLs

R-SFCLs are straightforward yet promising devices, leveraging the nonlinear resistivity and temperature-phase transition of superconductors. A block diagram of an R-SFCL device is illustrated in Fig. 1, where it is placed in series with the system to be protected and immersed in liquid nitrogen. During normal system operation, the current flowing through the superconductor remains below its critical value. While there may be some negligible ac loss [21], the equivalent resistance seen by the power systems remains minimal. However, in the event of a fault, when the grid current exceeds the critical current (J_c) of the superconductor, joule heating causes it to quench. Consequently, a non-negligible resistance emerges, limiting the fault current.

2.2. R-SFCL modeling using the thermal-electric analogy method

This section presents the modeling of R-SFCLs using second-generation high-temperature coated conductor YBCO tapes (Fig. 2(a)). We simplify heat transfer equations and address the electrical–thermal coupling using the thermal–electrical analogy method, which is ideal for large-scale grid simulations [22,23]. We calculate layer resistances theoretically based on material properties and dimensions, then use Ohm's law to find current distribution. Accurate transient behavior simulation requires calculating temperature rises during faults. Our model accounts for HTS material heating, heat exchange with the LN2 cooling bath, and interlayer heat transfers. These heat transfer equations are equivalent to an RC electric circuit (Fig. 2(b)), simplifying implementation with electromagnetic transient simulation software. The practical R-SFCL includes coils with superconducting YBCO tapes and parallel stainless-steel shunt resistors. To reduce inductance, we arrange HTS tapes in each module in an anti-parallel configuration. The device maintains superconductivity in LN2 at 77 K, with quench times typically under 1 ms. In our simulation, we vary the number of coils to adjust R-SFCL resistance from 5 Ω to 100 Ω to evaluate its impact on the CDP.

3. Working principle of current differential protective relay

Line current differential protection is a commonly used method for safeguarding transmission lines, rooted in Kirchhoff's Current Law (KCL).

In a differential relay setup, currents at each end of the protected component are closely monitored. Under normal conditions, KCL indicates that the sum of these currents should equal zero. An abnormality within the protected component or zone disrupts this equilibrium. This results in the sum of the currents deviating from zero. The relay detects this current differential. It then uses this differential as an indicator of a fault. This process is illustrated in Fig. 3.

Eq. (1) describes an internal fault (F_1), while (2) represents an external fault (F_2), or normal operation. Note that i_m, i_n, i_{f1} are instantaneous currents.

$$i_m + i_n = i_{f1} \tag{1}$$

$$i_m + i_n = 0 \tag{2}$$

The fundamental frequency component in the current is the power frequency component. This component is used to create a power frequency current differential, known for its stability and noise resistance. Note that I_D, I_m, I_n are phasors.

$$I_D = | \dot{I}_m + \dot{I}_n | \tag{3}$$

To enhance the reliability of the current differential relay and mitigate the impact of factors like distributed capacitance current, shunt reactor current, and the aperiodic component of short-circuit current in transmission lines, relay operation criteria often employ both differential and restraint currents:

$$| \dot{I}_m + \dot{I}_n | > I_{set} \tag{4a}$$

$$\frac{| \dot{I}_m + \dot{I}_n |}{| \dot{I}_m - \dot{I}_n |} > K \tag{4b}$$

Here, K represents the restraint coefficient, with a range of $0 < K < 1$, and I_{set} is the setting current [18].

4. Quantitative analysis of R-SFCL impact on CDPs

4.1. Mathematical analysis of the correlation between SFCL resistance, fault resistance, and CDP operation criteria

In this section, mathematical formulas relating fault resistance, SFCL resistance, and the CDP's operation criteria are developed using Fortescue's Theorem [24]. Given the non-linear nature of these formulas, which renders direct solutions infeasible, a graphical method in MATLAB is employed to visualize the correlation between these variables. The fault resistance acts as an indicator of the CDP's sensitivity, setting the foundation for subsequent analysis.

4.1.1. System overview

Consider a simplified power system as depicted in Fig. 4, which consists of two sources, labeled S_m and S_n. In this system, a short-circuit fault, designated as F, is introduced to model fault conditions. The fault has resistance R_f. The transmission line has a length of l, and the line impedance from M to the fault point is Z_{lm}, and from N to the fault point is Z_{ln}. Additionally, Z_{sm} and Z_{sn} correspond to the Thevenin equivalent impedance of sources M and N, respectively. $\dot{I}_M$ and $\dot{U}_M$ are current and voltage measured at point M. $\dot{I}_N$ and $\dot{U}_N$ are current and voltage measured at point N. The SFCL is characterized by a resistance of R_{sfcl}.

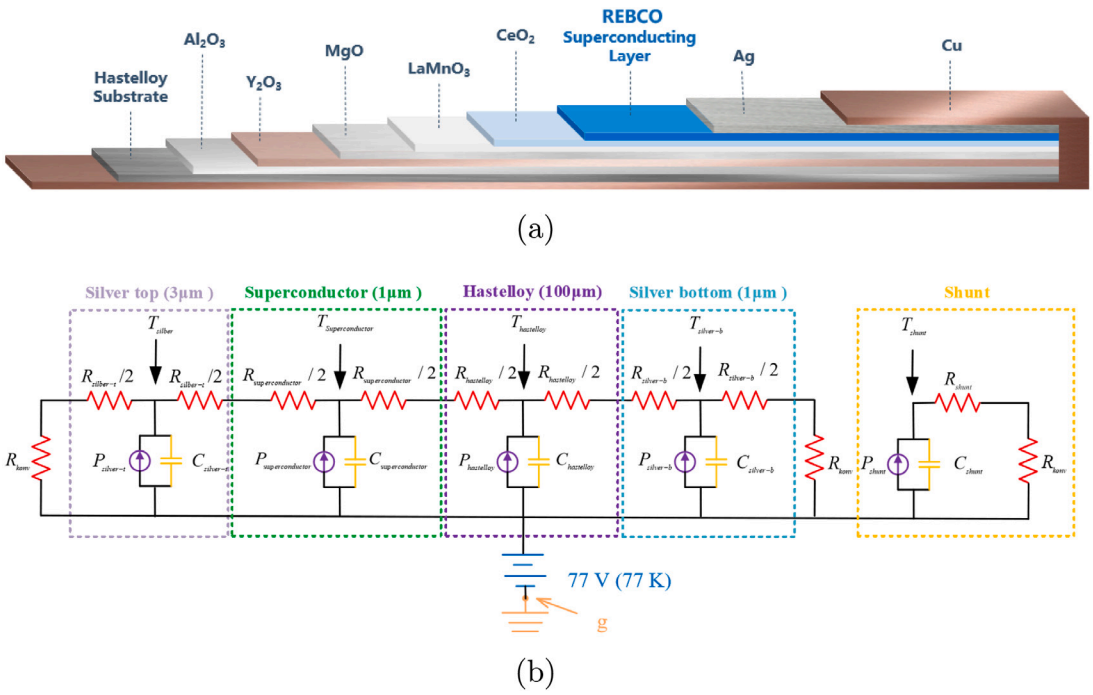

Fig. 2. (a) Hierarchical structure of commercial 2G YBCO tapes for SFCL (courtesy of Shanghai Superconductor Technology Co. Ltd.). (b) Thermal-electric circuit of each tape.

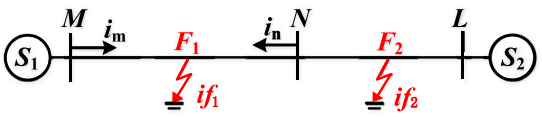

Fig. 3. Current differential protective relay.

4.1.2. System decomposition

Assuming an unbalanced fault, specifically a single-phase-to-ground fault (AG), the system can be represented as a superposition of a non-fault state and a fault additional state. The symmetrical components are illustrated in Fig. 5. Here, $\dot{I}_m$ and $\dot{I}_n$ represent the currents at terminals M and N, respectively. The subscripts $\gamma = 0, 1, 2$ represent zero, positive, and negative sequences.

For an AG fault, the boundary conditions are as follows:

$$\dot{I}_{Af} = \dot{I}_f \tag{5}$$

$$\dot{I}_{Bf} = 0 \tag{6}$$

$$\dot{I}_{Cf} = 0 \tag{7}$$

The symmetrical components for fault branches are calculated as follows for AG fault conditions:

$$\dot{I}_{Af} = \frac{\dot{I}_{1f} + \dot{I}_{2f} + \dot{I}_{0f}}{3} \tag{8}$$

$$\dot{I}_{Bf} = \frac{a^2\dot{I}_{1f} + a\dot{I}_{2f} + \dot{I}_{0f}}{3} \tag{9}$$

$$\dot{I}_{Cf} = \frac{a\dot{I}_{1f} + a^2\dot{I}_{2f} + \dot{I}_{0f}}{3} \tag{10}$$

Note that $a = e^{j2\pi/3}$.

For an AG fault, the boundary conditions are in symmetrical components:

$$\dot{I}_{1f} = \dot{I}_{2f} = \dot{I}_{0f} = \dot{I}_f \tag{11}$$

4.1.3. Fault current calculation

By combining the three sequence networks in Fig. 5, the fault current at fault point in sequence network $\dot{I}_f$ can be derived as follows, assuming $Z_{sm1} + Z_{lm1} = Z_{m1}$, $Z_{sn1} + Z_{ln1} = Z_{n1}$, $Z_{sm0} + Z_{lm0} = Z_{m0}$, $Z_{sn0} + Z_{ln0} = Z_{n0}$.

$$\dot{I}_f = \frac{\dot{U}_{1f} + \dot{U}_{2f} + \dot{U}_{0f}}{3R_f + 2(Z_{m1} + R_{sfcl})//Z_{n1} + (Z_{m0} + R_{sfcl})//Z_{n0}} \tag{12}$$

4.1.4. Relay operation

The relay operation involves calculating $\dot{I}_m$ and $\dot{I}_n$ as follows. $\dot{I}_L$ refers to the current under non-fault state in Fig. 4.

$$\begin{aligned}\dot{I}_m &= \dot{I}_{m1} + \dot{I}_{m2} + \dot{I}_{m0} + \dot{I}_L \\ &= \dot{I}_f \cdot C_1 + \dot{I}_f \cdot C_1 + \dot{I}_f \cdot C_0 + \dot{I}_L \\ &= \dot{I}_f(2C_1 + C_0) + \dot{I}_L\end{aligned} \tag{13}$$

in which $\dot{I}_{m1}$, $\dot{I}_{m2}$, $\dot{I}_{m0}$ are positive, negative and zero sequence currents at terminal M in sequence network of fault additional state. And C_1, C_0 denote the current diversions in positive network and zero network respectively.

$$\begin{aligned}\dot{I}_n &= \dot{I}_{n1} + \dot{I}_{n2} + \dot{I}_{n0} + \dot{I}_L \\ &= \dot{I}_f(1 - C_1) + \dot{I}_f(1 - C_1) + \dot{I}_f(1 - C_0) - \dot{I}_L \\ &= (3 - 2C_1 - C_0)\dot{I}_f - \dot{I}_L\end{aligned} \tag{14}$$

in which $\dot{I}_{n1}$, $\dot{I}_{n2}$, $\dot{I}_{n0}$ are positive, negative, and zero sequence currents at terminal N in sequence network of fault additional state.

$$C_1 = \frac{Z_{ln1} + Z_{sn1}}{Z_{sm1} + Z_{lm1} + R_{sfcl} + Z_{ln1} + Z_{sn1}} \tag{15}$$

$$C_0 = \frac{Z_{ln0} + Z_{sn0}}{Z_{sm0} + Z_{lm0} + R_{sfcl} + Z_{ln0} + Z_{sn0}} \tag{16}$$

$$\dot{I}_L = \frac{\dot{U}_M - \dot{U}_N}{Z_{sm1} + R_{sfcl} + Z_{lm1} + Z_{ln1} + Z_{sn1}} \tag{17}$$

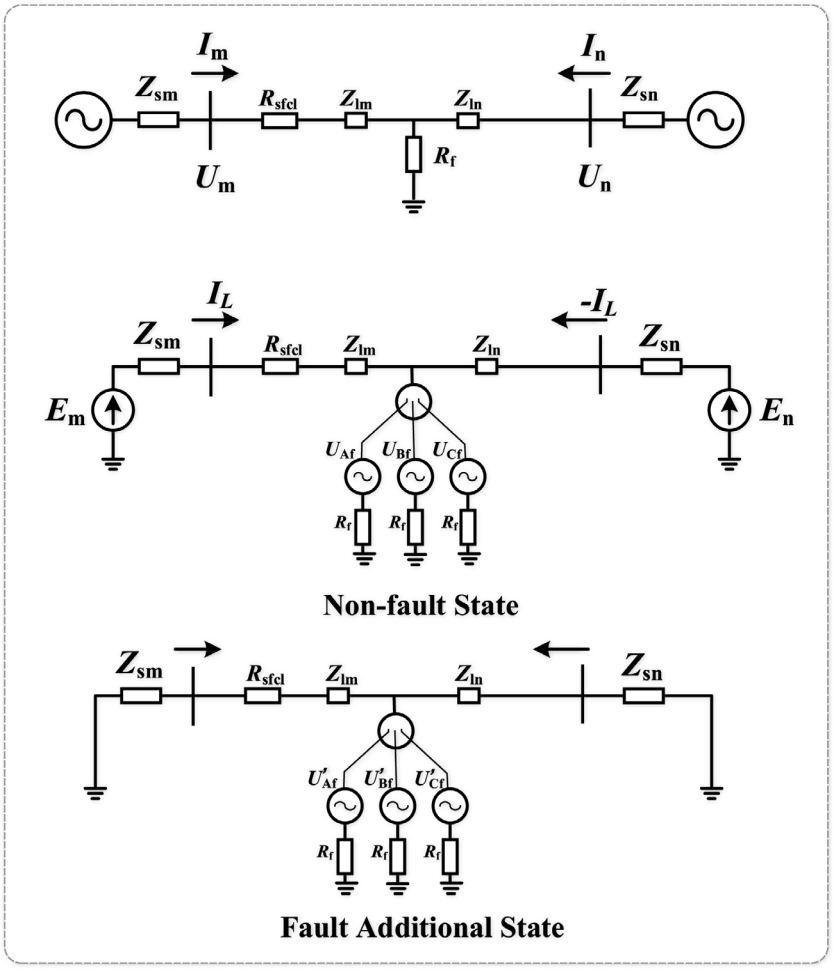

Fig. 4. Diagram of fault decomposition with R-SFCLs.

4.1.5. Differential and restraint currents

The differential current (I_d) and restraint current (I_r) are determined as follows:

$$I_d = |\dot{I}_m + \dot{I}_n| = 3\,|\dot{I}_f| \tag{18}$$

$$I_r = |\dot{I}_m - \dot{I}_n| = |\dot{I}_f(4C_1 + 2C_0 - 3) + 2\dot{I}_L| \tag{19}$$

The section concludes by solving Eq. (20) to analyze the impact of R-SFCL on the CDP:

$$f(R_f, R_{sfcl}) = \frac{|\dot{I}_m + \dot{I}_n|}{|\dot{I}_m - \dot{I}_n|} = k \tag{20}$$

Here, we designate the ratio k as the 'Practical Restraint Coefficient' (PRC). The solutions are graphically represented in Fig. 6, generated using Matlab, to showcase the interplay between fault resistance (R_f), SFCL resistance (R_{sfcl}), and the PRC.

4.2. Impact of SFCL on the sensitivity of the CDP relay

This subsection evaluates the sensitivity of the CDP relay in various fault scenarios, including high impedance fault (HIF) and low impedance fault (LIF). Additionally, the analysis explores the sensitivity enhancement with R-SFCLs and identifies a threshold beyond which this enhancement stabilizes.

The sensitivity of the CDP is determined by the highest permissible fault resistance (R_f) at which the relay operates correctly, as described in [25,26]. This analysis involves varying both R_f and R_{sfcl} within a range from 0 Ω to 100 Ω. Notably, the relationship between these parameters and the CDP's sensitivity, as shown in the graphs, does not follow a monotonic trend.

4.2.1. Low Impedance Fault (LIF)

In the presence of a low impedance fault (LIF) characterized by a fault resistance of 10 Ω, the integration of R-SFCLs with varying resistance values provokes interesting responses in the power system.

The differential current, representing the current difference between both terminals of the protected component, experiences a notable reduction of 35%. This reduction occurs due to the introduction of R-SFCLs, which increase their resistance values as fault conditions unfold.

The restraint current, which serves as a protective measure in the CDP, witnesses a substantial 133% increase. This increase can be attributed to the interaction between R-SFCLs and the fault conditions, causing restraint mechanisms to respond more firmly.

The parameter k, denoting the ratio of differential to restraint current as defined in Eq. (20), shows a distinctive pattern. Initially, it decreases from its initial value of 4.8 to approximately 1.3 as R_{sfcl}, the resistance of R-SFCL, increases to 100 Ω. However, k takes an unexpected turn, reaching a peak of 5.7 when R_{sfcl} is set at a lower value of 10 Ω. This peculiar behavior reflects the intricate interplay between R-SFCLs and fault scenarios.

The CDP is known to favor conditions with larger values of k, as this parameter reflects the system's ability to differentiate between normal and fault states. The introduction of R-SFCLs brings both positive and negative impacts within this parameter. While k tends to increase with R-SFCLs for low impedance faults, the operational impact on the

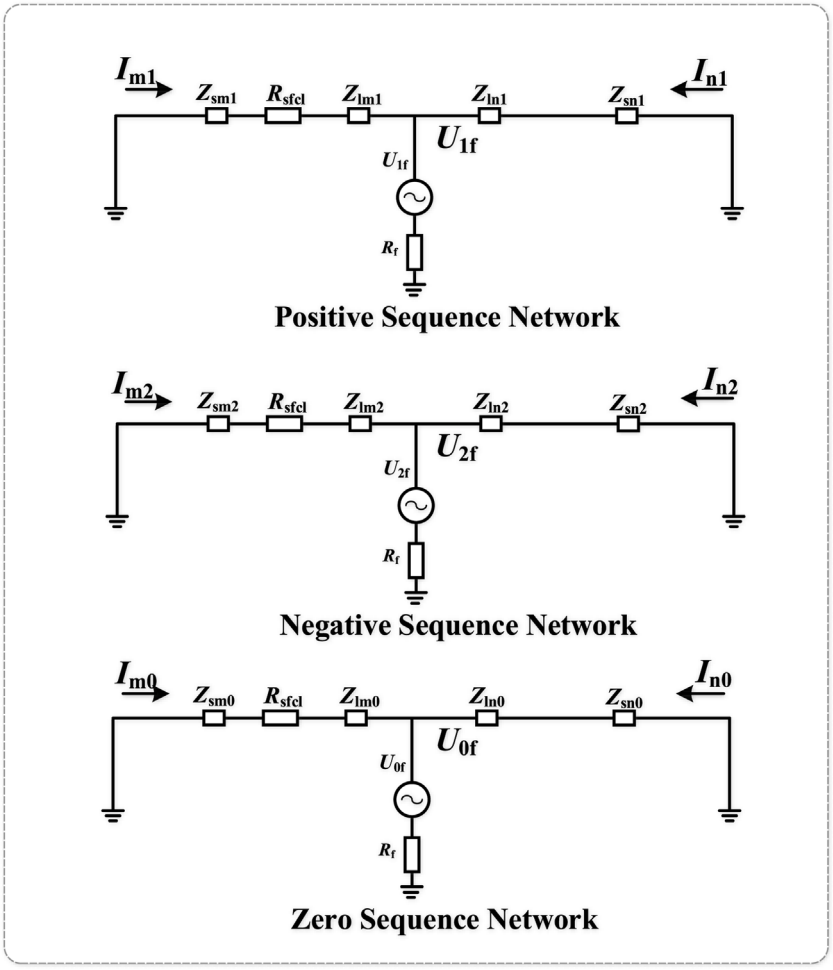

Fig. 5. Diagram of symmetrical components with R-SFCLs.

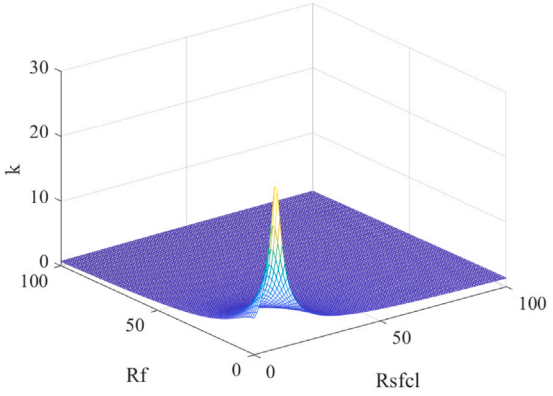

Fig. 6. The relationship between R_{sfcl}, R_f and k.

CDP is minimal. This is attributed to the significant margin between differential and restraint currents, leading to a substantial k value even with R-SFCLs.

4.2.2. High Impedance Fault (HIF)

In the case of a high impedance fault (HIF) scenario, defined by a fault resistance of 100 Ω, the integration of R-SFCLs with variable resistance values brings forth a distinct set of outcomes:

The differential current experiences a modest 1% increase. This increase is a result of R-SFCLs altering the fault conditions, leading to a slight augmentation in differential current.

Restraint current, which acts as a protective measure, undergoes a notable 28% reduction. The presence of R-SFCLs modifies the system's response, leading to a more relaxed restraint mechanism.

The parameter k demonstrates a significant increase, rising from 0.7 to approximately 0.97. This shift in k signifies a substantial alteration in the system's ability to distinguish between normal and fault states. The operational criteria of the CDP, typically governed by a customary restraint coefficient (K) set at 0.75, are profoundly influenced by the presence of R-SFCL, resulting in increased sensitivity.

This enhanced sensitivity directly correlates with the resistance value of R-SFCL. As the resistance of R-SFCL increases, the system becomes more responsive to high impedance faults, improving the reliability of the CDP.

4.2.3. Threshold sensitivity enhancement with R-SFCL

Interesting observation can be made when analyzing the sensitivity of the CDP in the context of internal faults and the integration of R-SFCLs. This phenomenon reveals a threshold beyond which the sensitivity of the CDP remains stable, regardless of the magnitude of the R-SFCL's resistance.

As depicted in Fig. 4, when the resistance value (R_{sfcl}) of the R-SFCL becomes larger, the current (I_m) flowing through the system decreases. At a certain point, the following conditions are met:

$$\dot{I}_n + \dot{I}_m \approx \dot{I}_n \tag{21}$$

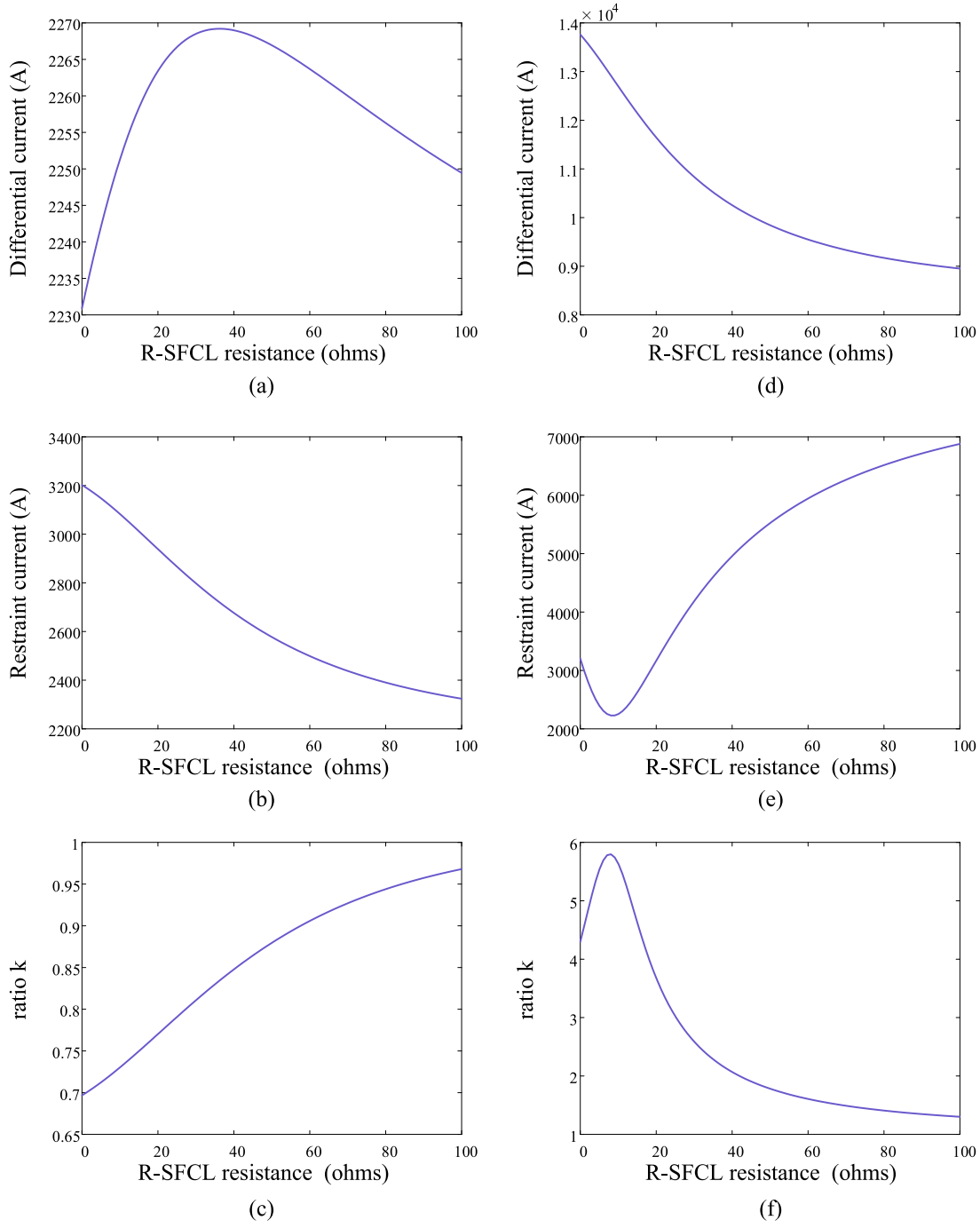

Fig. 7. The relationship between R_{sfcl} resistance and the CDP's operation criteria. Graphs (a)–(c) depict the system's behavior under Low-Impedance Faults, showing variations in differential current, restraint current, and the ratio k with different R_{sfcl} resistances. Graphs (d)–(f) depict High-Impedance Faults, illustrating changes in these parameters.

$$\dot{I}_n - \dot{I}_m \approx \dot{I}_n \tag{22}$$

In accordance with the parameter k introduced earlier, when these conditions hold true, k approaches the value of 1, surpassing the restraint coefficient (K). This key moment signifies that the criteria outlined in (4b) can be satisfied consistently.

Consequently, at this juncture, the sensitivity of the CDP becomes solely reliant on the condition stipulated in (4a), which dictates:

$$\dot{I}_n \geq I_{set} \tag{23}$$

Given that both $\dot{I}_n$ and I_{set} are constants with fixed values, it is evident that there exists an upper limit to the sensitivity that the CDP can achieve in the presence of R-SFCLs. Beyond this threshold, further increases in R-SFCLs' resistance no longer impact the sensitivity of the CDP, as it becomes constrained by the fixed values of $\dot{I}_n$ and I_{set}. This phenomenon underscores the need for careful consideration of the R-SFCLs parameters to optimize the performance of protective relays in power systems.

4.3. Impact of SFCL on the security of the CDP relay

When external faults occur, KCL remains valid regardless of whether an additional resistor is introduced. Consequently, the CDP will not malfunction. The introduction of R-SFCLs does not compromise the security of the CDP.

Table 1
Parameters of the power system.

Parameter	Value	Unit
Rated frequency	50	Hz
Source resistance	0.8929	Ω
Source inductance	32.58×10^{-3}	H
Rated voltage of S_M and S_N	230	kV
Phase angle of S_M and S_N	0° and 20°	–
Protected line length	100	km
Positive-Sequence resistance	0.01273	Ω/km
Zero-Sequence resistance	0.3864	Ω/km
Positive-Sequence inductance	0.9337×10^{-3}	H/km
Zero-Sequence inductance	4.1264×10^{-3}	H/km
Positive-Sequence capacitances	12.74×10^{-9}	F/km
Zero-Sequence capacitances	7.751×10^{-9}	F/km

Table 2
Simulation results for single-phase-to-ground fault (AG).

R-SFCL resistance value [Ω]	Fault resistance [Ω]/Sensitivity of the CDP	
	Without SFCL	With SFCL
5	68	72
10	68	75
20	68	81
30	68	83
40	68	83
50	68	83
100	68	83

4.4. Summary

The integration of R-SFCLs beneficially influences the performance of CDP relays. Specifically, R-SFCLs enhance the CDP's sensitivity towards internal faults. As the resistance of the SFCL increases, the operational criteria of the CDP are more readily met, increasing the likelihood of accurate relay activation. In the case of external faults, R-SFCLs demonstrate a neutral impact, maintaining the security integrity of the line current differential relay.

5. Case study

5.1. Modeling for the studied grid

The double-source three-phase power system, as depicted in Fig. 4, was simulated using MATLAB Simulink software for this study. A R-SFCL was strategically placed at bus M to reduce short-circuit currents. The current differential relay device installed on the S_m side was considered for analysis. Table 1 provides an overview of the parameters characterizing the power system.

5.2. Simulation results

5.2.1. R-SFCL's effect on CDP relays performance

In this section, we conducted a series of simulations to assess the sensitivity, dependability, and security of line current differential protection relays. These simulations were performed with and without R-SFCLs integrated into the grid. The R-SFCL was varied with resistance values ranging from 0 Ω to 100 Ω, with fault resistance varying from 1 Ω to 100 Ω. Various fault types were considered, including three-phase faults (ABC), single-phase-to-ground faults (AG), two-phase faults (BC), and two-phase-to-ground faults (BCG). We evaluated the sensitivity by analyzing the fault resistance and the presence of R-SFCLs. The simulation results on the sensitivity of CDP are summarized in Tables 2 to 5.

When a single-phase-to-ground fault occurs, as presented in Table 2, we observe that the maximum fault resistance at which the CDP can reliably operate is 68 Ω. However, this scenario changes significantly with the introduction of a 5 Ω R-SFCL into the system, leading to a notable increase in the maximum fault resistance to 72 Ω. Notably, this trend of improved sensitivity continues as the resistance of the R-SFCL is further increased to 10 Ω, 20 Ω, and 30 Ω, respectively.

Table 3
Simulation results for two-phase fault (BC).

R-SFCL resistance value [Ω]	Fault resistance [Ω]/Sensitivity of the CDP	
	Without SFCL	With SFCL
5	64	68
10	64	72
20	64	74
30	64	74
40	64	74
50	64	74
100	64	74

Table 4
Simulation results for two-phase-to-ground fault (BCG).

R-SFCL resistance value [Ω]	Fault resistance [Ω]/Sensitivity of the CDP	
	Without SFCL	With SFCL
5	76	80
10	76	83
20	76	90
30	76	91
40	76	91
50	76	91
100	76	91

Table 5
Simulation results for three-phase fault (ABC).

R-SFCL resistance value [Ω]	Fault resistance [Ω]/Sensitivity of the CDP	
	Without SFCL	With SFCL
5	76	79
10	76	82
20	76	89
30	76	90
40	76	90
50	76	90
100	76	90

Remarkably, the sensitivity enhancement reaches its peak when the R-SFCL's resistance is set to 30 Ω, allowing the CDP to operate reliably with a maximum fault resistance of 83 Ω. Beyond this point, increasing the R-SFCL's resistance to 100 Ω does not yield further improvements in sensitivity. This pattern is consistent across various fault scenarios, as observed in Table 2 and the corresponding tables for other fault types.

These findings underscore the effectiveness of R-SFCLs in enhancing the sensitivity of the CDP. The optimal sensitivity enhancement occurs when the R-SFCL's resistance is appropriately tuned, providing a valuable tool for enhancing the dependability of power system protection.

In summary, our simulations reveal that the deployment of R-SFCLs significantly enhances the sensitivity of CDP under different fault conditions, which highlights the potential of R-SFCLs as valuable components in modern power systems to ensure robust fault protection.

5.2.2. R-SFCL's effect on fault current suppression

In this section, we conducted simulations to evaluate the current-limiting effects of an R-SFCL with a resistance set to 30 Ω, across four types of faults in a power transmission line. The objective was to compare the current waveforms with and without the SFCL during fault events, as depicted in Fig. 8. The results underscore the SFCL's considerable impact in reducing fault current magnitudes in all tested scenarios. For the commonly occurring single-phase-to-ground fault, the SFCL effectively halved the fault current peak from approximately 6000 A to around 3000 A. In more complex fault scenarios, such as two-phase-to-ground and two-phase faults, the SFCL consistently capped the peak currents at under 4000 A, a significant decrease from the potential

Table 6
Scenario information for CDP performance evaluation.

Scenario	Fault Res.[a] (Ω)	SFCL Res.[b] (Ω)	CDP operation	
			W/O SFCL	W/ SFCL
I	20	30	Yes	Yes
II	85	5	No	No
III	85	30	No	Yes

[a] Fault Res. refers to Fault Resistance.
[b] SFCL Res. refers to SFCL Resistance.

peaks of nearly 7000 A. The most dramatic reduction was evident in the three-phase fault condition, the most severe of the fault types, where the SFCL was crucial in reducing an uncontrolled fault current that could reach up to 12 000 A, down to below 5000 A. These simulations underscore the SFCL's vital role in boosting system protection and reliability by effectively managing fault currents in power transmission lines.

5.3. Assessment of CDP sensitivity with R-SFCL integration under various fault scenarios

In the following section, we present a comprehensive analysis of three distinct scenarios to assess the impact of R-SFCLs on the CDP's operation. Scenario I represents a low impedance fault (LIF), while Scenarios II and III simulate high impedance faults (HIF). The waveforms depicting the differential current, restraint current, and the parameter k for Scenarios I and III are illustrated in Fig. 9. Due to their similarity, the graphs for Scenario II are omitted but align with the patterns observed in Scenario III.

Table 6 provides information about different scenarios used for evaluating the performance of the CDP system. The scenarios include variations in fault resistance and the presence of R-SFCLs. The table highlights whether the CDP operates correctly during fault conditions in each scenario.

5.3.1. Scenario I: Low Impedance Fault (LIF)

In Scenario I, a low impedance fault is considered. As shown in Fig. 9, upon the fault occurring, the differential current surges instantaneously from 0 A to 5481 A. However, with the introduction of an R-SFCL at 0.3 s, the differential current is promptly reduced to 4865 A. Once the faults are cleared, the differential current returns to its nominal zero value.

Simultaneously, the restraint current, initially at 2046 A, rises to 2554 A due to the fault and climbs further to 2736 A as a result of the R-SFCL's operation. This leads to a transient increase in the ratio k to 2.14 after 0.2 s, which subsequently stabilizes at 1.77 due to the presence of the R-SFCL. Importantly, in LIF scenarios, the CDP operates effectively as the conditions for its proper functioning are readily met. While the introduction of the SFCL negatively impacts the k ratio by reducing it, this effect remains inconsequential and does not compromise the CDP's performance.

5.3.2. Scenario II: High Impedance Fault (HIF) with low R-SFCL resistance

In Scenario II, a high impedance fault with a fault resistance of 85 Ω is considered, along with a low R-SFCL resistance of 5 Ω. When the fault occurs, the differential current reaches 2206 A. The subsequent introduction of the SFCL at 0.3 s reduces this current to 2163 A. Consequently, the k ratio increases from 0.68 to 0.70. However, the CDP malfunctions under these conditions as it struggles to meet the criteria defined by Eq. (4b). While the SFCL's presence contributes to a marginal improvement in k, the effect is limited due to the low resistance of the SFCL.

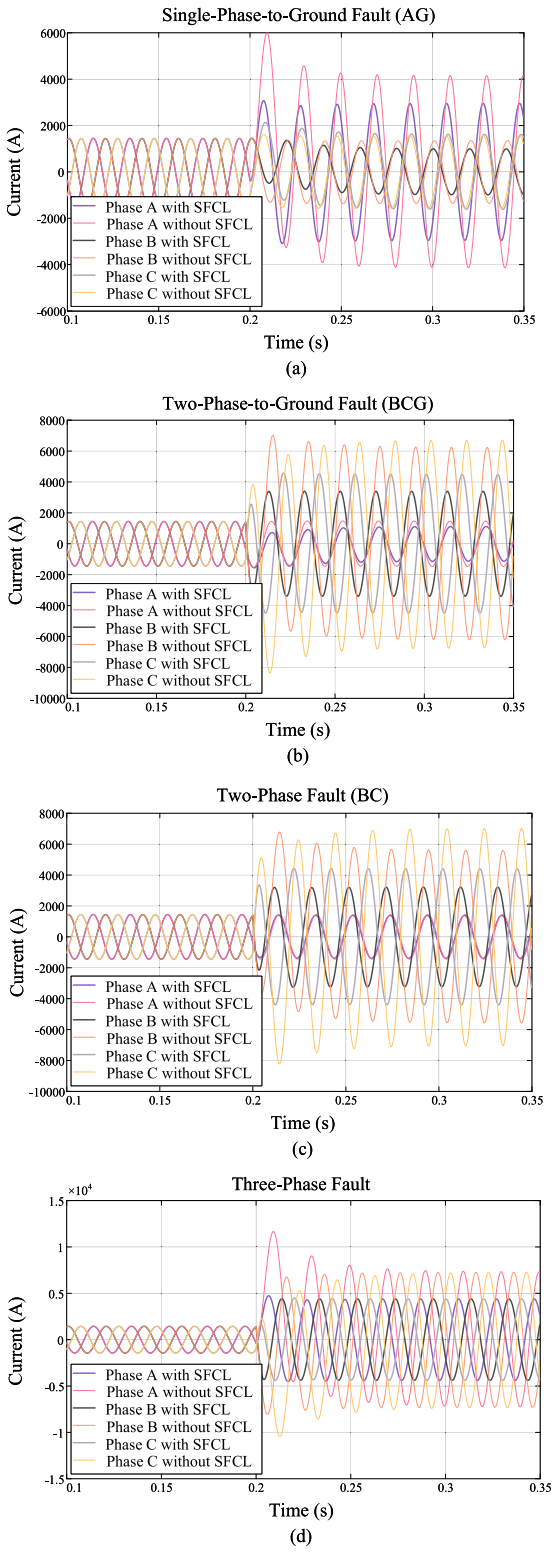

Fig. 8. Current limiting effect of SFCL for different types of faults. Graph (a) illustrates a single-phase to ground fault, (b) shows a two-phase to ground fault, (c) depicts a two-phase fault, and (d) represents a three-phase fault.

5.3.3. Scenario III: High Impedance Fault (HIF) with moderate R-SFCL resistance

In Scenario III, we examine a high impedance fault with a fault resistance of 85 Ω and a moderate R-SFCL resistance of 30 Ω. As

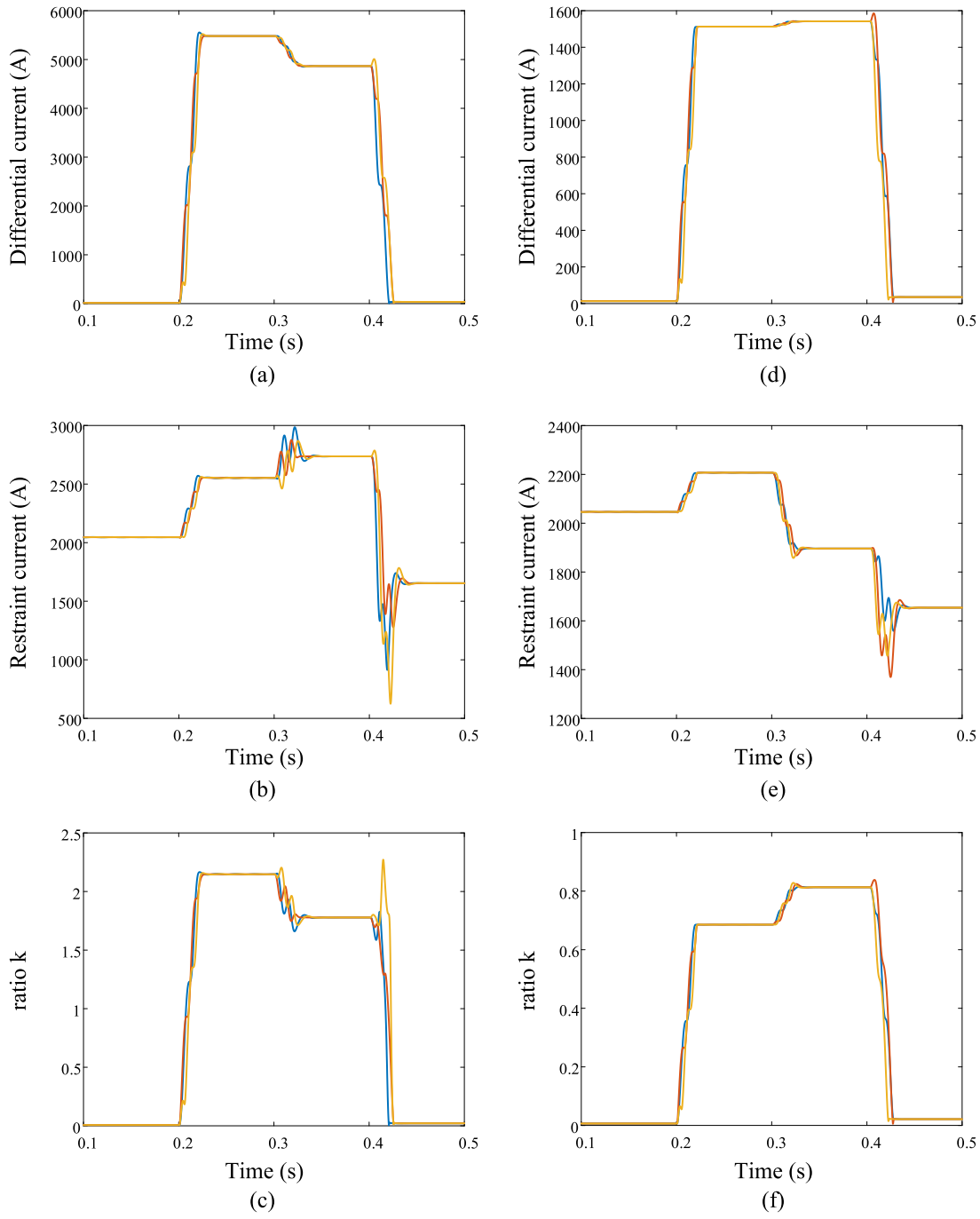

Fig. 9. The impact of integrating SFCL on the CDP's operation criteria. Graphs (a)–(c) depict the response to Low-Impedance Faults (Scenario I): Graph (a) shows differential current, Graph (b) restraint current, and Graph (c) the ratio k. Graphs (d)–(f) focus on High-Impedance Faults (Scenario III): Graph (d) illustrates differential current, Graph (e) restraint current, and Graph (f) the ratio k.

depicted in Fig. 9, the differential current rises to 1512 A at the beginning of the fault. With the R-SFCL activated at 0.3 s, the differential current further increases to 1542 A. This increment is more substantial compared to Scenario II, attributable to the higher resistance of the SFCL. For the restraint current, it initially surges to 2206 A during the inception of faults but subsequently decreases to 1896 A due to the quench of the SFCLs. Consequently, the k ratio undergoes a significant transformation with and without the SFCL. In the absence of the SFCL, between 0.2 s and 0.3 s of the fault duration, the value of k stays at 0.68, which is below the predefined criterion K. Conversely, when the SFCL is incorporated, k increases to 0.81 during the same period, surpassing the K threshold. This significant difference illustrates that the CDP misoperates without the SFCL under HIF conditions but functions correctly when R-SFCLs are employed. This underscores the favorable influence of SFCLs on enhancing the sensitivity and reliability of the CDP, aligning with the mathematical analysis.

The simulation results for these three scenarios align closely with the mathematical analysis, as indicated in Fig. 7.

5.4. Assessment of CDP security with R-SFCL integration

In the next phase of our investigation, the security of the line current differential protective relays were rigorously tested through the generation of external faults. Simulations were conducted under

various fault scenarios, encompassing both symmetrical and unsymmetrical configurations, as well as high and low impedance conditions. Remarkably, regardless of the fault configuration employed, the CDP system exhibited faultless and accurate operation in the presence of R-SFCLs. Notably, there were no observed instances of mal-operation.

These findings demonstrate that the introduction of R-SFCLs has no noticeable impact on the security of the CDP in mitigating external faults. This corroborates the analytical results presented in Section 3, further affirming the compatibility and robustness of the CDP system when integrated with R-SFCL technology.

These outcomes underscore the potential benefits of incorporating R-SFCLs into power systems, offering enhanced fault current management without compromising the fundamental security of protective relays.

6. Conclusion

This research provides an in-depth analysis of resistive superconducting fault current limiters (R-SFCLs) and their significant impact on line current differential relay operations, offering valuable insights for enhancing power system protection. Key findings include:

(1) Fault Current Restraint
R-SFCLs effectively restrain fault currents, demonstrating an inverse relationship with fault current magnitude, thus maintaining grid integrity.
(2) Enhanced Relay Performance
The integration of R-SFCLs substantially improves the sensitivity, dependability, and security of current differential relays, marking a significant advancement in grid protection.
(3) Universal Sensitivity Improvement
R-SFCLs consistently enhance relay sensitivity across various fault types, highlighting their versatility and broad applicability in diverse scenarios.
(4) Upper Limit Sensitivity
There is an upper limit to sensitivity enhancement with R-SFCLs, indicating a threshold beyond which no additional improvements are observed.

In summary, these findings overturns the common assumption that SFCLs impair protective relay functions. Instead, they demonstrate that R-SFCLs effectively coordinate with current differential protection, significantly improve grid protection.

CRediT authorship contribution statement

Qihuan Dong: Conceptualization, Data curation, Formal analysis, Funding acquisition, Investigation, Methodology, Project administration, Resources, Software, Supervision, Validation, Visualization, Writing – original draft, Writing – review & editing. **Haozong Wang:** Software. **Binshu Chen:** Investigation. **Ning Zhang:** Funding acquisition. **W.T.B. de Sousa:** Supervision. **Yilu Liu:** Supervision.

Declaration of competing interest

The authors declare no conflicts of interest regarding the research conducted and the submission of this paper. We affirm that this research was carried out without any external influence, financial or otherwise, that could be perceived as a potential conflict of interest.

Additionally, we confirm that no funding agency or organization with a vested interest in the results of this research has had any influence over the research design, data analysis, interpretation of findings, or the decision to submit this manuscript for publication.

We provide this statement to assure the integrity and transparency of our research work and to comply with the guidelines and standards set by the journal.

Data availability

The data that has been used is confidential.

Acknowledgments

This work was supported by the National Natural Science Foundation of China Youth Fund (52307023) and the Shuimu Tsinghua Scholar Program.

Funding and acknowledgments

This work was supported by the National Natural Science Foundation of China Youth Fund (52307023) and the Shuimu Tsinghua Scholar Program. We acknowledge the contributions of all collaborators and institutions that assisted in this research.

Ethical compliance

This research did not involve human participants, animal subjects, or data derived from either, and thus did not require ethical approval. All research was conducted in accordance with the ethical standards of the scientific community.

References

[1] Dong Q. Study of superconducting fault current limiters in power systems (Ph.D. thesis), University of Cambridge; 2019.
[2] Safaei A, Zolfaghari M, Gilvanejad M, Gharehpetian GB. A survey on fault current limiters: Development and technical aspects. Int J Electr Power Energy Syst 2020;118:105729.
[3] Melhem Z. High temperature superconductors (HTS) for energy applications. Woodhead Publishing; 2012.
[4] Hobl A, Goldacker W, Dutoit B, Martini L, Petermann A, Tixador P. Design and production of the ECCOFLOW resistive fault current limiter. IEEE Trans Appl Supercond 2013;23(3):5601804.
[5] Noe M, Hobl A, Tixador P, Martini L, Dutoit B. Conceptual design of a 24 kV, 1 kA resistive superconducting fault current limiter. IEEE Trans Appl Supercond 2012;22(3):5600304.
[6] Tixador P, Bauer M, Bruzek C-E, Calleja A, Deutscher G, Dutoit B, Gomory F, Martini L, Noe M, Obradors X, Pekarčíková M, Sirois F. Status of the European union project FASTGRID. IEEE Trans Appl Supercond 2019;29(5):1–5.
[7] Tixador P, Akbar A, Bauer M, Bocchi M, Calleja A, Creusot C, Deutscher G, Gomory F, Noe M, Obradors X, Pekarčíková M, Sirois F. Some results of the EU project FASTGRID. IEEE Trans Appl Supercond 2022;32(4):1–6.
[8] Eckroad S. Superconducting power equipment: Technology watch 2012. Technical update 1024190, Electric Power Research Institute; 2012.
[9] Hyun O-B, Yim S-W, Yu S-D, Yang SE, Kim W-S, Kim H-R, Lee G-H, Sim J, Park K-B. Long-term operation and fault tests of a 22.9 kV hybrid SFCL in the KEPCO test grid. IEEE Trans Appl Supercond 2011;21(3):2131–4.
[10] Hong H, Su B, Niu GJ, Cui JB, Tian B, Li Q, Wang LZ, Wang ZH, Zhang K, Xin Y. Design, fabrication, and operation of the cryogenic system for a 220 kV/300 MVA saturated iron-core superconducting fault current limiter. IEEE Trans Appl Supercond 2014;24(5):1–4.
[11] The national “863 Project” high-voltage superconducting current limiter has been successfully developed. URL http://www.xinhuanet.com//politics/2017-06/29/c_1121236525.htm.
[12] Song M, Ma T, Sheng C, Dai S, Zhong L, Duan X, Li L. The parameter design and system simulation of 160-kV/1-kA resistive-type superconducting DC fault current limiter. IEEE Trans Appl Supercond 2019;29(5):1–6.
[13] Dong Q, de Sousa WT, Geng J, Zhang X, Zhang H, Shen B, Coombs T. Influences of the resistive SFCL on the incremental power frequency relay of transmission lines. IEEE Trans Appl Supercond 2019;29(2):1–7.
[14] Firouzi M, Gharehpetian G, Mozafari B. Bridge-type superconducting fault current limiter effect on distance relay characteristics. Int J Electr Power Energy Syst 2015;68:115–22.
[15] Rebizant W, Solak K, Brusilowicz B, Benysek G, Kempski A, Rusiński J. Coordination of overcurrent protection relays in networks with superconducting fault current limiters. Int J Electr Power Energy Syst 2018;95:307–14.
[16] Li C, Wang S, Li B, Wu Q, Zhu J, Zhang H, Xin Y. Impacts of a flux-coupling SFCL on the overcurrent protection for distribution system with infeed. Int J Electr Power Energy Syst 2023;149:109036.
[17] Anderson PM, Henville C, Rifaat R, Johnson B, Meliopoulos S. Power system protection. John Wiley & Sons; 2022.

[18] He J. Principles of power system relay protection. 4th ed.. China Electric Power Press; 1980.
[19] Kraemer H-P, Bauer A, Frank M, van Hasselt P, Kummeth P, Wohlfart M, Schacherer C, Arndt T, Janetschek T. ASSiST - a superconducting fault current limiter in a public electric power grid. IEEE Trans Power Deliv 2022;37(1):612–8.
[20] IEEE guide for application of digital line current differential relays using digital communication. IEEE std C37.243-2015, 2015, p. 1–72.
[21] Buckel W, Kleiner R. Superconductivity: fundamentals and applications. John Wiley & Sons; 2008.
[22] Thermal–electrical analogy for simulations of superconducting fault current limiters. Cryogenics 2014;62:97–109.
[23] Silva R, Mafra G, Sotelo G, Fortes M, Trillaud F, Guillen D. Impact of superconducting fault current limiters on delayed current zeros in industrial power systems. Int J Electr Power Energy Syst 2023;145:108594.
[24] Fortescue CL. Method of symmetrical co-ordinates applied to the solution of polyphase networks. Trans Amer Inst Electr Eng 1918;XXXVII(2):1027–140.
[25] Gilany M, Malik O, Hope G. A digital protection technique for parallel transmission lines using a single relay at each end. IEEE Trans Power Deliv 1992;7(1):118–25.
[26] Dambhare S, Soman SA, Chandorkar MC. Adaptive current differential protection schemes for transmission-line protection. IEEE Trans Power Deliv 2009;24(4):1832–41.